Available online at www.sciencedirect.com

SCIENCE @ DIRECT®

Surface Science 540 (2003) 274–284

SURFACE SCIENCE

www.elsevier.com/locate/susc

# Deposition of lead iodide films on Rh(1 0 0) electrodes from colloidal solutions—the effect of an iodine adlayer

Chia-Huei Yang [a], Shueh-Lin Yau [a,*], Liang-Jen Fan [b], Yaw-Wen Yang [b,*]

[a] *Department of Chemistry, National Central University, ChungLi 320, Taiwan, ROC*
[b] *Synchrotron Radiation Research Center, Hsinchu 300, Taiwan, ROC*

Received 8 February 2003; accepted for publication 22 May 2003

## Abstract

The growth of $PbI_2$ precipitates on single crystal substrates from colloidal solutions has been investigated with in air scanning tunneling microscopy and synchrotron-based X-ray photoelectron spectroscopy. The $PbI_2$ growth on Rh(1 0 0) results in nano-clusters with lateral dimensions between 30 and 60 Å, consistent with earlier reports. However, the growth of $PbI_2$ on a well-ordered iodinated Rh(1 0 0), denoted as $(\sqrt{2} \times \sqrt{2})R45°$-I, leads to atomically smooth $PbI_2$ films having a hexagonal symmetry with lattice constant identical to the bulk value of 4.5 Å. The heteroepitaxy is believed to be effected by the atomic iodine monolayer that helps to accommodate large lattice mismatch between $PbI_2$ and Rh surface with short-range van der Waals interaction.

*Keywords:* Scanning tunneling microscopy; X-ray photoelectron spectroscopy; Lead; Halides; Epitaxy; Growth; Iodine; Rhodium

## 1. Introduction

Lead iodide ($PbI_2$) is a wide bandgap semiconductor ($E_g = 2.32$ eV) and has been a semiconductor material for use in solid state X-ray and gamma-ray detectors [1,2]. The thin film fabrication of lead iodide material is expected to open up its application. Heavy metal iodides are structurally similar to transition-metal dichalcogenides. Their basic structure repeat unit is a hexagonally close-packed layer of metal ion sandwiched between two layers of iodide ions. For lead iodide, the sequence of I–Pb–I planes thus defines a molecular layer. The unit cell dimension is $a = 4.557$ and $c = 6.979$ Å [3]. Each atomic plane in the molecular layer is consisted of strongly bonded atoms of the same element, but the bonding between adjacent molecular layers is due to weak, van der Waals force [4]. Owing to this structural anisotropy, it is possible to grow layer-structured $PbI_2$ materials over a large lateral dimension [5].

The structure of small-scale $PbI_2$ materials has been investigated by transmission electron microscopy (TEM) and atomic force microscopy (AFM) [6,7]. Both results indicate preferential formation of single-layered, platelet-like nanoclusters with lateral dimensions ranging from 1 to 6 nm, depending on the solution concentration. TEM data also point to the existence of stacking

---

[*] Corresponding authors. Tel.: +886-3-4227151-5909; fax: +886-3-4227664.

*E-mail address:* philyau@cc.ncu.edu.tw (S.-L. Yau).

0039-6028/$ - see front matter © 2003 Elsevier B.V. All rights reserved.
doi:10.1016/S0039-6028(03)00839-2

faults i.e., a few percent of polytypism of 4H, 6R, and 12R present besides predominant 2H structure [6]. AFM results reveal an averaged $10 \pm 1$ Å height for $PbI_2$ clusters deposited on mica, suggesting a seemingly large interlayer expansion by as much as 40% [7]. Meanwhile, an ab initio calculation predicts that in-plane lattice constant can decrease by 10% accompanied by the increase of interlayer distance [8]. It suffices to say that the structure of the supported $PbI_2$ thin film is still not completely certain.

One major benefit expected from the current nano-materials research is the ability to engineer the bandgap of semiconductor materials through quantum confinement effect. Previous studies successfully demonstrated a blueshift of UV absorbance peaks for the decreasing size of $PbI_2$ clusters, produced from a simple solution preparation procedure [5–12]. When engineering this class of bandgap materials, the importance of controlling individual property and assembling them in an orderly fashion cannot be overstated. As a layer-structure material, the growth of $PbI_2$ film is subject to some certain constraints. For instance, the film thickness can only be increased at a multiple of 7 Å, the thickness of a complete charge-neutralized I–Pb–I layer. As for in-plane dimension, whether there exists a size-propensity for the $PbI_2$ clusters is still a subject of discussion due to the uncertainty in assigning the observed optical transitions [6]. Due to a large disparity in the surface free energies between dichalcogenide and the metal substrate, it will be of great interest to engineer a heteroepitaxy by altering the free energy of the metal surface through the adsorption of foreign materials [13].

In the present paper, we report a joint scanning tunneling microscopy (STM) and X-ray photoelectron spectroscopy (XPS) study of the thin $PbI_2$ films grown from solution onto different substrates. STM is utilized to characterize the real-space atomic structures of the films. High-resolution synchrotron based XPS work addresses the chemical structure and species distribution of the lead iodide precipitate. We found a striking difference of $PbI_2$ growth upon changes of substrates—from nano-clusters occurring on a clean Rh(1 0 0) to an atomically smooth, crystalline film on ordered iodine-pre-dosed Rh(1 0 0). The van der Waals interaction derived from the pre-dosed iodine adlayers is believed to be responsible for the ensuing growth of atomically flat $PbI_2$ film.

## 2. Experimental

### 2.1. Preparation of iodine-coated Rh(1 0 0) substrate

The Rh(1 0 0) electrodes were made by melting one end of an ultrapure Rh wire ($\phi = 0.8$ mm) with a hydrogen and oxygen torch. With a high melting point of 1923 °C and the readiness for oxidation, it was rather difficult to melt the rhodium to prepare high-quality single crystal Rh beads. The *as-prepared* Rh beads have a mean diameter of $\approx$2 mm. To deposit iodine overlayers, we annealed the Rh(1 0 0) electrode with a hydrogen torch for 5 min and then quickly transferred the electrode into an iodine-containing glass cell. During the operation, the whole setup was purged constantly with ultrapure nitrogen gas.

The iodine molecules dissociatively adsorb on the Rh(1 0 0) surface. The number of iodine adlayers and their surface morphology depended sensitively on the iodine deposition conditions such as partial pressure of iodine, $N_2$ flow rate, size and temperature of Rh electrodes, the distance between the Rh and iodine sources, etc. No single recipe for growing iodine monolayer could be exactly specified. However, a higher flow rate and a larger separation from the iodine source to the electrode tended to favor the growth of iodine monolayer. Typically, we placed the annealed Rh(1 0 0) electrode 1 mm away from the iodine source under a high $N_2$ flow rate. This procedure was usually successful in making well-ordered iodine adlattices. Once the Rh electrodes were coated with iodine atoms, their surfaces appeared hydrophobic and essentially passivated toward further oxidation or adsorption of organic contaminants in air. Similar iodine pretreatment has been applied for growing ordered films on noble transition-metal electrodes of Pt, Ir, Pd, and Au [14–17].

### 2.2. Preparation of $PbI_2$ solutions

All the chemicals, including lead nitrate, potassium iodide, and acetonitrile were of ultrapure grade and used without further purification. Triply distilled Millipore water was used to prepare all solutions. We adopted the procedure reported in the literature to prepare $PbI_2$ nanoparticles [5–9]. This method involved adding 5 ml 0.01 M $Pb(NO_3)_2$ to 100 ml actonitrile, followed by the injection of an aliquot of 2.5 ml 0.05 M KI under constant stirring. The resultant solution appeared to be pale yellow but transparent. An iodine-modified Rh(1 0 0) electrode was then dipped into this $PbI_2$ solution for 1 min or longer, depending on the type of material to be studied. The Rh(1 0 0) electrode was then dried with a nitrogen steam before mounting onto the STM cell.

According to several previous studies, this preparation procedure produced $PbI_2$ nano-crystallites with lateral dimensions grouped around 1.2, 1.8, and 2.9 nm [5]. These species were thought to be responsible for the prominent absorption features in the optical spectrum at 3.42, 3.95, and 4.80 eV, respectively. In addition to acetonitrile, a number of organic solvents, for example, 2-propanol and pyridine, were tested as the co-solvent in making $PbI_2$ colloidal solutions. It appeared that polyiodide ions and metallic hydroxide species formed in wet chemistry could cause complications in characterizing $PbI_2$ nano-clusters [11]. Furthermore, pyridine could replace iodide inside the coordination sphere of $Pb^{2+}$ ions and thus modified the optical properties of the nano-clusters [12].

### 2.3. STM measurements in air

The STM was a Nanoscope-E (Santa Barbara, CA) and the tip was made of tungsten (diameter 0.3 mm) prepared by electrochemical etching in 2 M KOH. Cleaning was done by rinsing with water and acetone prior to use. The scanner was an A-head from digital instruments. The maximal scan size was $500 \times 500$ nm and the piezo was calibrated against a highly oriented pyrolytic graphite sample. Thermal drift appeared to be a main obstacle in obtaining the correct measurements of interatomic spacing. Thus, we normally used a scan rate of 40 Hz in high-resolution scans to minimize the influence of thermal drift. The spatial measurements from STM results typically had an error of ±5%.

### 2.4. X-ray photoelectron spectroscopy

All the photoemission data were acquired from an ultra-high vacuum (UHV) end station hooked up to BL12A wide range spherical grating monochromator beamline (WR-SGM) at Synchrotron Radiation Research Center. This unique beamline was equipped with a set of six spherical gratings to deliver soft X-ray photons with energy ranging from 15 to 1500 eV. The mu-metal UHV chamber housed a differentially pumped sputter ion gun for sample cleaning, an angle-integrated VG CLAM4 energy analyzer, an angle-resolved VG ADES 400 energy analyzer, and a load-lock sample transfer mechanism. A combined energy resolution of the beamline and energy analyzer was estimated to be better than 0.2 (0.5) eV for 200 (700) eV photon energy in use here. All the XPS spectra presented here were first normalized to photon flux by dividing recorded XPS signal with photocurrent derived from a gold mesh situated in front of the sample. Binding energy scale in all the spectra was calibrated against three Rh core levels spanning a wide energy range: Rh $4p_{3/2}$ at 47.27, Rh $3d_{5/2}$ at 307.2, and Rh $3p_{3/2}$ at 496.5 eV. [18,19]. Because the Rh single crystal electrode employed for STM measurement was rather small, $\approx$3 mm diameter, another larger Rh(1 0 0) single crystal with a diameter of 10 mm was used for photoemission measurement. This single crystal was cleaned by the flame-annealing and the good crystallinity was confirmed by STM before the deposition of the $PbI_2$ thin films.

## 3. Results and discussion

### 3.1. In air STM imaging of iodine adlayers on Rh(1 0 0)

Fig. 1a shows a constant-current, topography scan of a Rh(1 0 0) electrode coated with one monolayer of iodine atoms. Well-defined features of steps and terraces, typical of single crystal

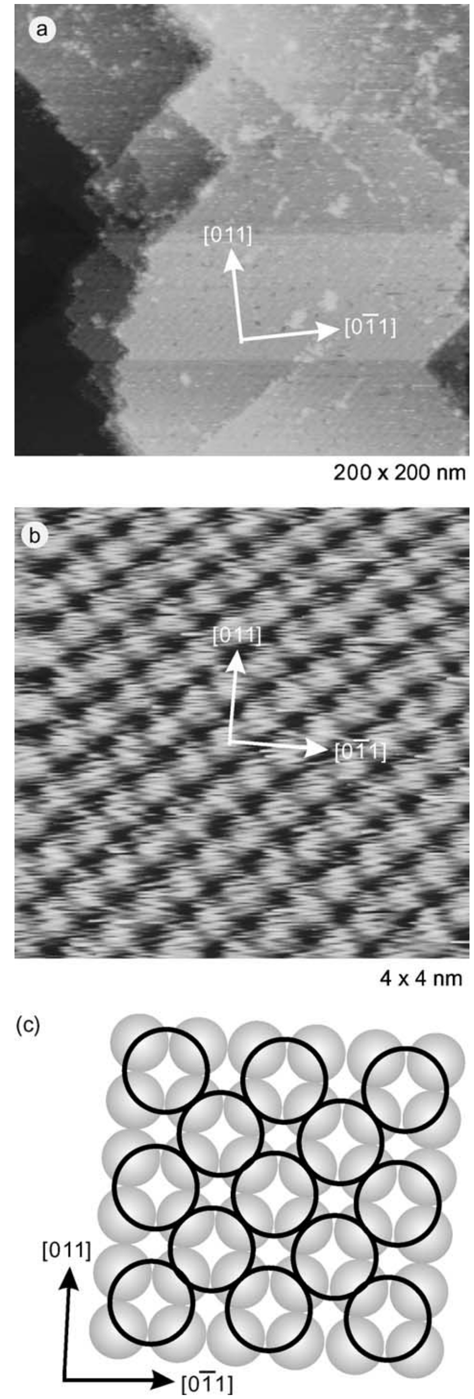

Fig. 1. (a) In air STM image of an iodine-modified Rh(1 0 0) surface, where the white arrow marks a dislocation defect. (b) Atomically resolved image of (a). (c) A ball model corresponds to the atomic arrangement in (b).

surfaces, are obvious. The steps are found to intersect at a near 90° angle, a feature commonly observed on a fcc(1 0 0) surface. Nearly all the steps are parallel to the [0 0 2] and [0 2 0] directions, along which the close-packed atomic rows of $(\sqrt{2} \times \sqrt{2})R45°$-I lie (vide infra). Fig. 1b shows the atomically resolved STM image of the terrace, indicating a highly ordered square array, attributable to the uppermost iodine adlayer. The close-packed atomic protrusions are aligned 45°—rotated from the atomic rows ([0 1 1] and $[0\,\bar{1}\,1]$ directions) of the Rh(1 0 0) substrate. The spacing measured between two nearest-neighboring iodine atoms is 0.38 nm, which corresponds nicely to the theoretical value ($\sqrt{2}$ times the spacing of Rh atom 0.268 nm). Thus, this STM result indicates the formation of a $(\sqrt{2} \times \sqrt{2})R45°$ iodine lattice, consistent with that reported previously [20].

This iodine structure is highly ordered with very few vacancy defects within the adlattice. It is worthwhile mentioning that for all the studies of iodine adsorption on Pt(1 1 1), Pt(1 0 0) and Ir(1 1 1) [14–16], vapor phase dosing always produces fewer vacancy defects and domain boundaries in the iodine overlayers than those produced by adsorption from KI solutions [21]. All the atomic features appear to be equally bright with the corrugation of 0.04 nm, a typical value found for iodine adatoms chemisorbed on transition-metal surfaces like Pt, Rh, Ir, etc. Fig. 1c presents a ball model for the Rh(1 0 0)-$(\sqrt{2} \times \sqrt{2})R45°$-I structure with all iodine atoms residing at identical 4-fold hollow sites. This model necessitates similar intensity for all iodine atoms in the STM image, as indeed observed in Fig. 1b.

In addition, the STM results reveal an unusual surface feature, marked by a white arrow in Fig. 1a. A careful examination reveals that it stretches for nearly 60 nm before vanishing into the terrace. Consequently, this feature would be better defined as a dislocation defect, rather than a step ledge, although it exhibits a height difference of 0.25 nm. In comparison, we hardly notice this type of defect on iodine-modified Pt(1 1 1) and Rh(1 1 1) electrodes prepared in a similar manner [14–16]. The cause of this unique phenomenon is not clear at present. These dislocation defects persisted after the deposition of $PbI_2$ films.

As noted by previous researchers, the layer thickness of iodine on Rh(1 0 0) largely hinged on the conditions under which they were deposited. A van der Waals interaction is presumed to be responsible for the growth of iodine multilayers. Detailed structural investigation will be presented elsewhere. The formation of iodine multilayers on noble transition-metals, such as Ir and Rh, is a rule, rather than an exception [15,16].

### 3.2. STM imaging of the surface morphology of $PbI_2$ films

As described in Introduction Section, the interaction among dissimilar Pb and I layers in $PbI_2$ is of strong electrostatic force in origin, but the interlayer interaction among a complete, charge-neutralized $PbI_2$ monolayer is due to weak, van der Waals force. The data, including those not presented here, show the formation of iodine multilayer interacting via weak van der Waals force is possible. We will now explore the possibility of growing an atomically smooth $PbI_2$ film supported on iodine monolayer through a utilization of van der Waals interaction. Fig. 2a shows an STM image obtained for an I-modified Rh(1 0 0) electrode soaked for 1 min in a $PbI_2$-containing solution that is also comprised of water and acetonitrile. The smoothness of the film is evident, and the image is different from those for iodine monolayer and iodine multilayer. Several questions can be raised regarding this finding. What chemical species are responsible for the observed image and what kind of the depth distribution these species have? What happens to the atomic iodine layer laid down prior to the $PbI_2$ deposition? Does this iodine layer become incorporated into I–Pb–I layer structure or does this iodine layer exist as a separate entity from I–Pb–I? Obviously, the answers to these questions cannot be provided by STM alone. We thus digress slightly and invoke synchrotron-based high resolution XPS data to shed light on these questions.

### 3.3. XPS measurements

Fig. 3a shows an XPS survey spectrum for the $PbI_2$ thin film taken with a photon energy of 700 eV. The short solution immersion time was used to ensure a $PbI_2$ monolayer structure that allows the I–Rh interface to be examined. The spectrum

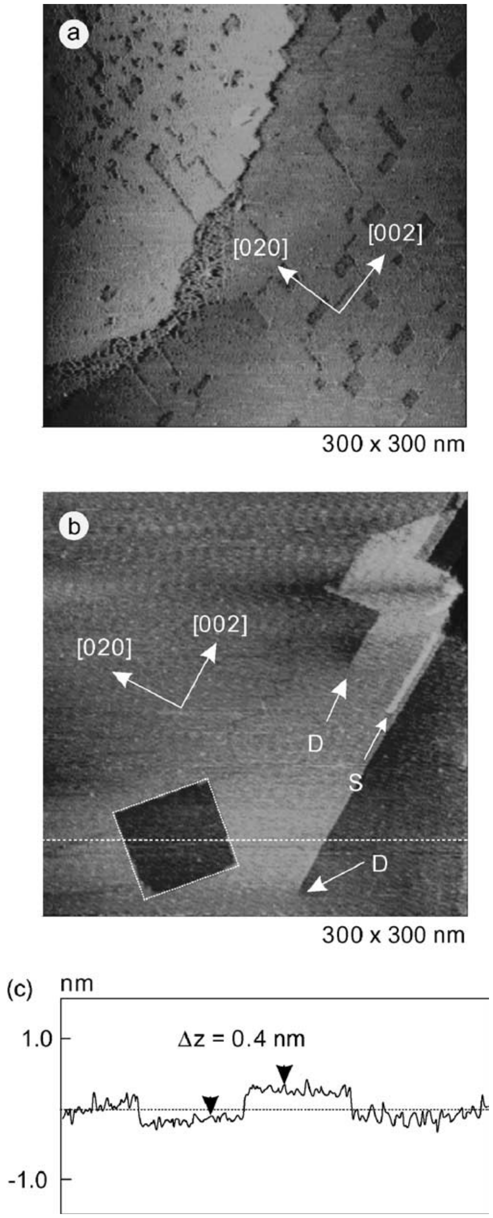

Fig. 2. (a) In air STM topographic scan showing the surface morphology of a $PbI_2$ film deposited on an iodine-modified Rh(1 0 0). (b) Another topography scan obtained in a separate experiment, where D and S, respectively, represent dislocation and isolated islands. (c) A cross-section profile along the dotted line in (b).

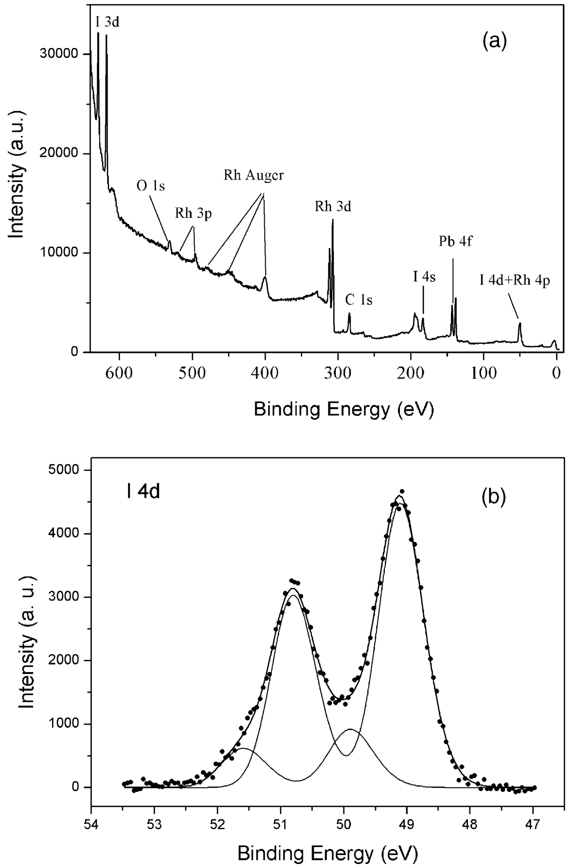

Fig. 3. (a) A survey XPS spectrum for $PbI_2$ thin film taken at a photon energy of 700 eV. The peak assignments are designated with the labels displayed nearby. (b) High-resolution I 4d core level spectrum for $PbI_2$ thin film. The spectrum was acquired at 40° emission angle with 200 eV photons. A non-linear least squares fit reveals the presence of two I components denoted in thin lines. The resultant curve is expressed as solid line that runs through raw data (symbols). A minute contribution by the substrate Rh $4p_{5/2}$ signal at 47.3 eV can become noticeable for an emission angle approaching surface normal.

contains a series of peaks with the labels of the peak assignments included for the ease of reference. It is found that, besides a small amount of carbon and oxygen contaminants, the $PbI_2$ thin film is relatively clean even prepared from a somewhat contaminant-prone solution environment. The near complete absence of K 2p doublets at 293 and 295.8 eV is in accord with the prediction based on the large solubility product constants of KI and $KNO_3$. The I $3d_{5/2}$ and Pb $4f_{7/2}$ core levels appear at 618.8 and 138.4 eV, respectively, in good agreement with the literature values of 619.5 and 138.7 eV for the bulk $PbI_2$ [18,19]. When the $PbI_2$ thin film is briefly annealed to 200 °C in vacuum, the $PbI_2$ film decomposes to evolve iodine into the gas phase while leaving behind a metallic Pb species, evidenced by its binding energy shift to 136.8 eV. This XPS result confirms the formation of $PbI_2$.

High-resolution I 4d photoemission measurement was performed to discern the iodine species because of the involvement of both iodine and iodide in the preparation method. I 4d rather than I 3d core level is preferred because of its narrower lifetime width [22] and a better energy resolution of the beamline at the lower energy end. Fig. 3b shows an I 4d core level spectrum for the as-prepared $PbI_2$ thin films taken at a photon energy of 200 eV. A non-linear least squares fitting is performed using a constant background in conjunction with a line shape function generated by a convolution of the Gaussian function with the Doniach–Sunjic function broadened by a finite lifetime. The spin orbit splitting in the doublet is fixed at 1.70 eV and a branching ratio of the doublet is optimized at 0.65, close to its statistical value of 0.67. In a given spectrum, the Gaussian with ($\Gamma_G$), Lorentzian width ($\Gamma_L$) and Doniach–Sunjic asymmetric parameter ($\alpha$) are allowed to vary in the fits but are constrained to be the same for all the peaks. A consistent set of parameters emerges from fitting the spectra of four different angles. The best fit parameters are as follows: $\Gamma_G = 0.672$ eV, $\Gamma_L = 0.233$ eV, and $\alpha = 0.035$, in line with earlier reports of iodine adsorption on Ag(1 1 1) and Ge(1 1 1) [22,23]. Most importantly, the fitting reveals the presence of two I components with a major peak at I $4d_{5/2} = 49.1$ eV and a minor one at I $4d_{5/2} = 49.9$ eV. The intensity ratio between two peaks is 4:1.

The structure of as-prepared $PbI_2$ thin film is discussed in light of the finding of two I 4d core levels. The I $4d_{5/2}$ core level of 49.1 eV is attributed to the iodide bonded to Pb ions, due to the larger screening of negative ion. In comparison, the I $4d_{5/2}$ core level of 49.9 eV is assigned to the chemisorbed iodine atom, with binding energy higher than that found for $I_{ad}$ on Ag(1 1 1), 48.9 eV [22]. The support of this assignment comes from the intensity analysis. For a substrate covered by a homogeneous adsorbate layer of thickness $d$, the attenuation of photoelectron signal for the substrate can be described as

$$I_s = I_{0,s}e^{-d/\lambda_s \cos\theta}$$

where $I_s$ and $I_{0,s}$ are the intensities of photoelectron peaks for the adsorbate-covered substrate and clean substrate, respectively; $\theta$ is the angle between the substrate surface normal and electron collection direction; and $\lambda_s$ is the inelastic mean-free-path that refers to the photoelectrons traversing through the said adsorbate. If one unreconstructed $PbI_2$ monolayer is formed on top of $(\sqrt{2} \times \sqrt{2})$-$R45°$-I, the elemental ratio between iodide and iodine is expected to be around 1.6:1, based on the respective lattice constants. In the aforementioned equation, the exact value of the $\lambda$ term is always plagued with some uncertainty. For the present case, the situation is further complicated by the presence of mixed Pb and I layers. Specifically, $\lambda$ parameter now refers to how the photoelectrons of specific energy are attenuated as they pass through I and Pb layers. This parameter is not readily available and we thus model the $PbI_2$ on $I_{ad}$ system as a homogeneous medium of constant layer spacing $l$. A layer-attenuation factor, $e^{-l/\lambda}$, can be immediately calculated as 0.72, or $\lambda/l = 3$, from the observed 4:1 intensity ratio ($(1 + 0.72^2)/0.72^3 = 4.1$). For lower iodide layer, a value of $0.72^2$ is expected since it locates below the top iodide and the Pb layers. Similar arguments apply to the bottom iodine layer and give rise to a value of $0.72^3$ for this layer. The distance from $I_{ad}$ layer to the top $I^-$ layer, $3l$, should be close to the $c$-axis value of the bulk $PbI_2$, namely, 7 Å. Thus, the $\lambda$ value is also equal to 7 Å, a very realistic value [24], given the rather crude approximation used. Moreover, under the constraint of a short $\lambda$ parameter, a significant fraction of $I_{ad}$ signal can be still observed, suggesting the thin nature of the $PbI_2$ film. It is most likely to be a monolayer film because each additional $PbI_2$ layer will increase the film thickness by a hefty amount of 7 Å. In brief summary, XPS data unambiguously show the formation of $PbI_2$ on Rh–I surface. The high-resolution I 4d data indicate that $I_{ad}$ layer exists as a separate entity and on top of which a single $PbI_2$ monolayer forms. This picture of $PbI_2$ thin film is in accord with the STM results that we shall return to now.

### 3.4. STM imaging of the atomic structures of $PbI_2$ films

It is critical to select a proper set of parameters when performing STM imaging. Strong interaction between the scanning probe and the surface can result in the etching of the $PbI_2$ films. On the one hand, we usually employed a bias voltage of more than 500 mV and a feedback current of lower than 5 nA to minimize the etching effect. On the other hand, we also explored the etching phenomenon to measure the thickness of the monolayer and multilayer $PbI_2$ film because the removal of filmy $PbI_2$ proceeded in a layer-by-layer fashion. An artificially created step is typically 0.7 nm deep, which agrees with the lattice constant along the $c$-axis of $PbI_2$. Although a previous ab initio study claims that both intralayer contraction and interlayer expansion occur for the $Pb_6I_{12}$ cluster [9], we found no evidence supporting this claim for the thin film materials. For layered semiconductors, the phenomenon of tip-induced etching is ubiquitous. Reported systems include $WSe_2$, $MoS_2$, $HgI_2$, $PbI_2$, and others [25–28]. The etching event can be due to mechanical or electrochemical force; however, we will refrain from a further discussion because this issue falls outside the present context.

By and large, the deposition of $PbI_2$ does not lead to a major change in the surface morphology. Well-defined steps and terraces preexisting on the iodine-modified Rh substrate are still preserved. The uniformity of the terraces seems to suggest that the $PbI_2$ film is ordered. Indeed, high-resolution scans of the $PbI_2$ terraces reveal clearly resolved atomic features, as shown in Fig. 4a and b.

The imaging parameters are 500 mV and 5 nA and these atomically resolved structures are stable against prolonged imaging, unless the bias voltage decreases to 200 mV or lower. The symmetry of these two structures is essentially hexagonal, despite the presence of some inevitable distortion (±5°), owing to the thermal drift of the piezo tube.

The average nearest neighbor spacing of 0.45 nm is slightly larger than the van der Waals diameter (0.43 nm) of an iodine atom but agrees quite well with the lattice constant of bulk $PbI_2$. Moreover, the image in the Fig. 4a features radiative hexagonal trenches, denoted by the dotted lines, along the closed-packed atomic rows of the hexagonal array. The trenches are mainly the dislocation defects that separate two neighboring hexagonal domains.

Fig. 4b shows the presence of two rotational domains that are separated by a winding domain boundary highlighted by a dotted trace. These two domains are rotated 45° with respect to each other and one of their closed-packed atomic rows are parallel to the close-packed direction of $(\sqrt{2}\times\sqrt{2})R45°$-I, i.e., [0 1 0]. The films are all atomically flat and exhibit a long-range order. Fig. 4c shows a model of the $PbI_2/(\sqrt{2}\times\sqrt{2})R45°$-I system, where $PbI_2$, maintaining at its bulk lattice constant, stacks on top of the atomic iodine layer. Atomic iodine layer is represented with solid circles and, for clarity, only the lower iodide layer (hollow circles) is depicted in the model with the upper iodide and $Pb^{2+}$ layer sandwiched in-between omitted. Due to the lattice mismatch between the hexagonal $PbI_2$ structure and the square lattice of the I–Rh(1 0 0) substrate, it is concluded that an incommensurate adsorption structure results, leading to a corrugated surface. (Sentences in red are misplaced, kind of odd here, considering deletion? If so, change However to Moreover in the next sentence) However, from the atomic smoothness of the $PbI_2$ film, it can be argued that the films are formed through a sequential deposition of $Pb^{2+}$ and $I^-$ layers, rather than a deposition via $PbI_2$ particles. A deposition via particle accumulation will inevitably lead to films exhibiting considerable surface roughness.

One ordered $PbI_2$ domain is highlighted and reproduced in Fig. 5a. Also presented in Fig. 5b and c are the profiles of two sectional cuts along the solid and dotted lines in Fig. 5a. The height difference between markers 1 and 2 in Fig. 5b is 0.11 nm, suggesting that the vacancy defect is one atom deep and a small corrugation of 0.04 nm is usually obtained. Fig. 5c shows the corrugation along the dotted line and the resultant profile

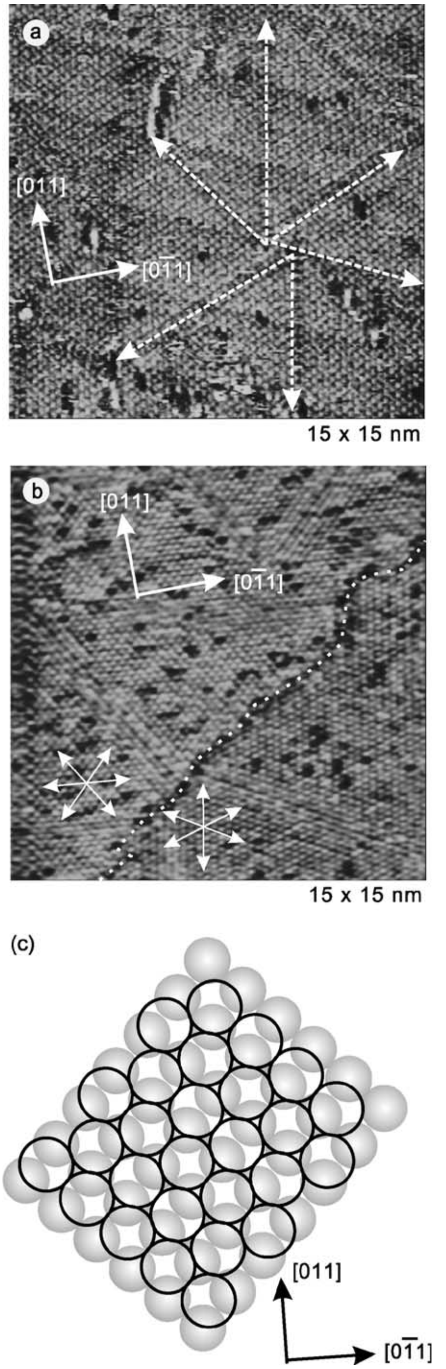

Fig. 4. (a) and (b) are two atomically resolved STM images, showing the arrangements of the uppermost iodide layer at different locations of the sample. The ball model in (c) depicts the relationship between the iodine adlayer and $PbI_2$ film. The imaging parameters are 500 mV and 5 nA.

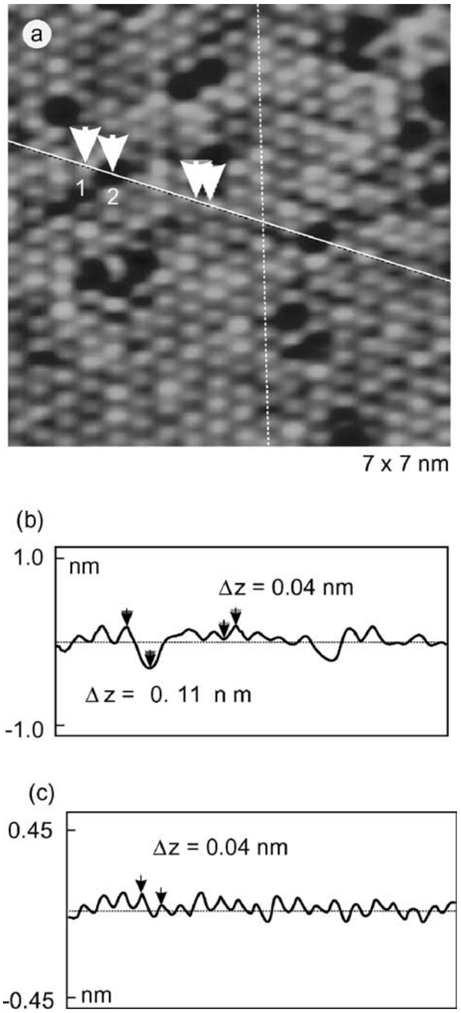

Fig. 5. (a) An STM image highlighting the atomic arrangement in the $PbI_2$ film, where (b) and (c) are corrugation profiles along the solid and dotted lines in the image.

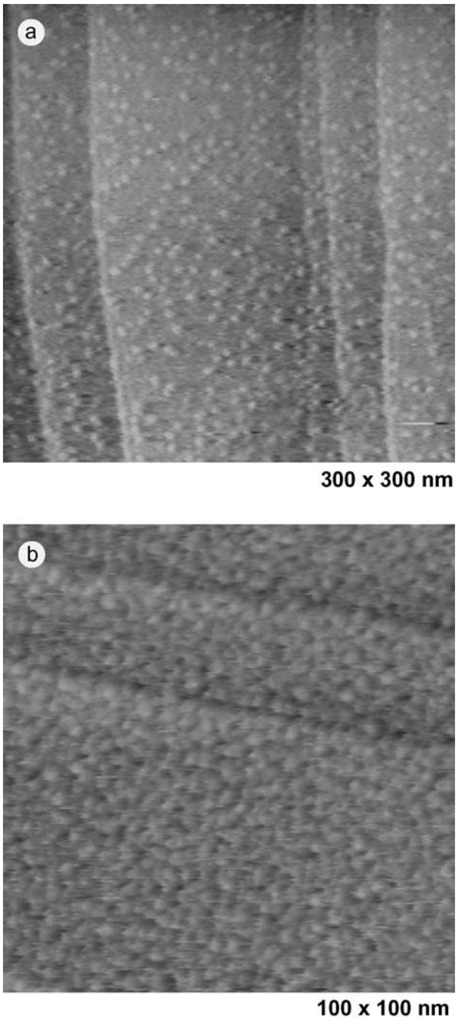

Fig. 6. In air STM images of Rh(1 0 0) surfaces exposed to a $PbI_2$-containing water and acetonitrile colloidal solution for 2 (a) and 5 (b) min.

provides a typical intensity variation along a closed-packed direction. This difference in atomic corrugation can stem from unlike chemical nature or registries of adsorbates. In the present situation, the atomic features are due to the uppermost layer of iodide ions of the $PbI_2$ film. Because it is not possible for all the iodide ions to have identical registries with respect to the underlying square lattice of $(\sqrt{2} \times \sqrt{2})R45°$-I, the presumed substrate net. The corrugations of iodide ions thus reflect the physical height difference among atoms in the film.

To discern the role played by the chemisorbed iodine layer in governing the growth of lead iodide films on Rh(1 0 0) surfaces, we examined the $PbI_2$ deposited onto a bare Rh(1 0 0) electrode with the STM. Fig. 6 shows two topographic scans obtained for two individual samples prepared in separate experiments. The results in a and b were obtained for Rh(1 0 0) soaked in $PbI_2$-containing colloidal solutions for 2 and 5 min, respectively. Compared to the surface morphology of iodine-modified Rh(1 0 0) in Fig. 5, the surfaces in both cases appear much rougher, featuring protruding islands preferentially located at the terraces. The averaged diameter of protruding features is about 30 Å in a and 60 Å in b. The relative corrugation heights of these nano-clusters are 7 and 2.5 Å for the case of a and b, respectively. The former corresponds to the ideal height for a $PbI_2$ layer, but the origin of the latter is difficult to determine. Theoretically, it is possible to use STM to discern the chemical natures of the protruding islands. The spectroscopy mode, invoking the $dI/dV$ relationship, allows the differentiation between these two species. In reality, the presence of water layer on the $PbI_2$ sample and/or the tip prohibits us from obtaining reproducible results. However, an additional observation that these protruding features can be dissolved by water rinsing suggests that these features are due to water-soluble $PbI_2$, instead of water-insoluble iodine.

The dramatic difference between $PbI_2$ thin films deposited on bare Rh(1 0 0) and on iodine-modified Rh(1 0 0) is to be discussed here. The $PbI_2$ film grown on the iodine-modified Rh surface exhibits atomic-scale smoothness, whereas the $PbI_2$ grown on Rh surface shows nano-sized clustering features. We speculate on the following reasons for this difference. Previous studies show iodine atoms covalently bond to Ni [29], Cu [30] and Rh [31] substrates, as evidenced by the fact that iodine-metal bond length is equated to the sum of iodine covalent radius and the metal metallic radius. Room temperature adsorption of molecular iodine on Rh(1 0 0) leads to a saturation structure of $(\sqrt{2} \times \sqrt{2})R45°$-I at a coverage of 0.5 ML and the distance between two nearest-neighboring iodine atoms is 3.80 Å, in-between covalent diameter (2.67 Å) and van der Waals diameter of 4.3 Å. Saturation coverages of iodine atoms on a metal surface are thought to be limited by the iodine–iodine repulsive interaction rather than bonding interactions with the metal surface. Our observation of surface passivation once iodine layer is adsorbed on various metals agrees with the earlier reports in which iodine layer also passivates highly reactive semiconductor surfaces like Si [32] and Ge [23]. Taken together, we argue that the overlayer growth on top of iodine layer seems to proceed via van der Waals interaction. The van der Waals force is weak and short-range and the iodine atoms, located at identical 4-fold hollow sites, essentially shield the charge corrugation due to the metal surface. The smoothened surface corrugation can then facilitate the layer growth of $PbI_2$ because the interlayer interaction among completed $PbI_2$ unit is also van der Waals force. In contrast, the layer growth of $PbI_2$ on bare Rh(1 0 0) will be difficult, given the presence of lattice mismatch between $PbI_2$ lattice and the Rh substrate as well as the large atomic corrugation of the Rh surface.

Because of the non-directional character of ionic bonding in these films, the spatial arrangements of ions are theoretically dominated by factors, such as lattice matching between the films and the substrate and the electronic properties of the films. There are many studies addressing the geometric effect. For example, the heteroepitaxial growth of ionic films of $MgCl_2$ on several transition-metal surfaces has been examined by using low energy electron diffraction [33]. It is concluded that the geometric matching between substrate and adsorbate plays a pivotal role in controlling the growth of the $MgCl_2$ films. Similar findings are reported for heteroepitaxial growth of CuCl and CuBr, zinc-blend structure ionic compounds, on MgO-(0 0 1) with rock-salt structure [34]. In addition to this geometric effect, Tasker first hypothesized the need to have zero dipole moment perpendicular to a substrate as a necessary condition for the formation of a stable ionic crystal surface [35]. This idea seems to be applicable in the present case because of the involvement of a completely charge-neutralized $PbI_2$ layer. Based on the STM results in Figs. 4 and 5, it is believed that the most stable configuration of the films can consist of $I^-$–$Pb^{2+}$–$I^-$ tri-layers sequentially stacked normal to the surface normal. Although each layer is charged, there is no net dipole moment in the surface normal.

## 4. Conclusion

A pre-dosed iodine adlayer on Rh(1 0 0) is found to exert a marked effect on the deposition of $PbI_2$ from colloidal solutions prepared with water and acetonitrile. Atomically resolved STM images reveal a highly ordered $(\sqrt{2} \times \sqrt{2})R45°$ iodine overlayer with atomically flat terraces spanning 100 nm wide. This structure serves as the substrate onto which a crystalline $PbI_2$ film is deposited via a simple immersion process. STM imaging reveals a hexagonal lattice with a lattice constant of 0.45 nm, attributable to the uppermost anionic iodide layer of $PbI_2$ because the $Pb^{2+}$ layer lying under the iodide layer cannot be directly imaged. In view of lattice-matching requirement during thin film growth, the formation of a thin film with a hexagonal symmetry on a 4-fold symmetric structure is somewhat unexpected. The XPS result unambiguously establishes a stacked structure in which the $PbI_2$ layer is located on top of the iodine layer. The iodide anions of the $PbI_2$ layer is believed to interact with the pre-dosed iodine through van der Waals force. In contrast, dipping a bare Rh(1 0 0) electrode in $PbI_2$-containing colloidal solutions results in a deposition of nano-flakes. The flakes are about 7 Å in height, suggesting a single layer thickness. The lateral dimensions of the flakes vary between 30 and 60 Å.

## Acknowledgements

This work is supported by the National Science Council of the Republic of China under contract no. NSC 90-2119-M-008-002. We thank K.S. Liang of SRRC for a fruitful discussion on the growth mode of thin film.

## References

[1] K.S. Shah, J.C. Lund, F. Olschner, P. Bennett, J. Zhang, L.P. Moy, M.R. Squillante, Nucl. Instrum. Meth. Phys. Res. Sect. A 353 (1994) 85.

[2] J.P. Ponpon, M. Amann, Thin Solid Films 394 (2001) 276.

[3] O. Madelung (Ed.), Semiconductors: Other Than Group IV Elements and III–V Compounds, Springer-Verlag, Berlin, 1992.

[4] G. Harbeke, E. Tosatti, RCA Rev. 36 (1975) 40.

[5] C.J. Sandroff, D.M. Hwang, W.M. Chung, Phys. Rev. B 33 (1986) 5953.

[6] E. Lifshitz, M. Yassen, L. Bykov, I. Dag, R. Chaim, J. Phys. Chem. 98 (1994) 1459.

[7] R. Mu, Y.S. Tung, A. Ueda, D.O. Henderson, J. Phys. Chem. B 100 (1996) 19927.

[8] M.M. Marino, M. Sawamura, W.C. Ermler, C.J. Sandroff, Phys. Rev. B 41 (1990) 1270.

[9] K. Mallik, T.S. Dhami, Phys. Rev. B 58 (1998) 13055.

[10] D. Sarid, T. Henson, L.S. Bell, C.J. Sandroff, J. Vac. Sci. Technol. 6 (1988) 424.

[11] I.O. Micic, L. Zongguan, G. Mills, J.C. Sullivan, D. Meisel, J. Phys. Chem. 91 (1987) 6221.

[12] Y. Wang, N. Herron, J. Phys. Chem. 91 (1987) 5005.

[13] R. Kern, G. Le Lay, J.J. Metois, Basic mechanisms in the early stages of epitaxy, in: E. Kaldis (Ed.), Current Topics in Materials Science, vol. 3, North Holland, Amsterdam, 1979, p. 131.

[14] B.C. Schardt, S.-L. Yau, F. Rinaldi, Science 243 (1989) 1050.

[15] L.M. Yang, S.L. Yau, J. Phys. Chem. 104 (2000) 1769.

[16] K. Itaya, Prog. Surf. Sci. 58 (1998) 121.

[17] X.P. Gao, M.J. Weaver, J. Am. Chem. Soc. 114 (1992) 8544.

[18] V.I. Nefedov, Y.V. Salyn, X. Keller, Zh. Neorg. Khim. 24 (1979) 2564.

[19] J.F. Moulder, W.F. Stickle, P.E. Sobol, K.D. Bomben, in: J. Chastain (Ed.), Handbook of X-ray Photoelectron Spectroscopy, Perkin-Elmer Corp., Eden Prairie, MN, 1992.

[20] R.T. Hiehsen, Ph.D. thesis, Purdue University, 1990.

[21] J. Inukai, Y. Osawa, M. Wakisaka, K. Sashikata, Y.-G. Kim, K. Itaya, J. Phys. Chem. 102 (1998) 3498.

[22] G.K. Wertheim, S.B. DiCenzo, D.N.E. Buchanan, Phys. Rev. B 25 (1982) 3020.

[23] M. Göthelid, G. LeLay, C. Wigren, M. Björkqvist, U.O. Karlsson, Surf. Sci. 371 (1997) 264.

[24] W.S.M. Werner, Surf. Interface Anal. 18 (1992) 217.

[25] B.A. Parkinson, J. Am. Chem. Soc. 112 (1990) 7498.

[26] E. Delawski, B.A. Parkinson, J. Am. Chem. Soc. 112 (1990) 7498.

[27] H.P. Lang, B. Erler, A. Rossberg, M. Piechotka, E. Kaldis, H.J. Guntherodt, J. Vac. Sci. Technol. B 14 (1996) 970.

[28] M.A. George, K.-T. Chen, W.E. Collins, A. Burger, D. Nason, L. Boatner, J. Vac. Sci. Technol. 14 (1996) 1096.

[29] R.G. Jones, S. Ainsworth, M.D. Crapper, C. Somerton, D.P. Woodruff, Surf. Sci. 152 (1985) 443.

[30] P.H. Citrin, P. Eisenberger, R.C. Hewitt, Phys. Rev. Lett. 45 (1980) 1948, Erratum 47 (1981) 1567.

[31] A.G. Shard, V.R. Dhanak, A. Santoni, Surf. Sci. 429 (1999) 279.

[32] A.W. Stephens, M.A. Green, Sol. Energy Mater. Sol. Cells 45 (1997) 255.

[33] D.H. Fairbrother, J.G. Roberts, G.A. Somorjai, Surf. Sci. 399 (1998) 109.

[34] A. Yanase, Y. Segawa, Surf. Sci. 329 (1995) 219.

[35] P.W. Tasker, J. Phys. C: Solid State Phys. 12 (1979) 4977.